4

Granular Flows in Rotary Kilns

We have stated in Chapter 2 that axial flow of a particulate material in a rotary kiln must pass through the active layer. Chemical reaction, for example the dissociation of limestone in lime kilns, are initiated and take place there. Hence any quantification of the transport processes in a rotary kiln must begin with establishing the depth of this layer. This notwithstanding, only a handful of quantitative predictions for the depth of the active layer have appeared in the literature, probably because of the complexity of analyzing granular flows. Granular flow is a form of two-phase flow consisting of particles and interstitial fluid (Hunt, 1997). When sheared, the particulates may either flow in a manner similar to a fluid, or resist the shearing like a solid. The dual nature of these types of flows makes them difficult to analyze. There is no deterministic description of the granular flow behavior unless it is approximated by the laws governing conventional non-Newtonian fluid flow as has been done for slurry flows. However, such an approach does not adequately represent the flow behavior because the flow properties such as consistency and the power law exponent associated with non-Newtonian flows are not easily measurable in rotary kilns. The early attempts to model granular flow in kilns include Pershin (1988), who, using results from a series of experimental trials on a small rotary drum, was able to mathematically model the shape of a cascading bed and, as a result, predicted the boundary between

the active layer and the plug flow region with a reasonable degree of accuracy. Pershin's model was based on the fundamental principles of the equilibrium theory that hypothesizes that, if motion is steady in a gravity field, then the system should assume the position of minimum potential energy and, as a result, the system's mass must be reduced by moving some of the material beyond the boundary of the system. The model was unique at the time because, for the first time, it provided explicit mathematical expressions that could be used to calculate the centroid of the plug flow region, its area, and consequently the mass of material in the active layer. Although the model fell short of predicting the flow in the active region, where the material is in some form of kinetic motion, an application of mass balance in the transverse plane could offer knowledge of the average mass velocity in the active layer. Unfortunately, Pershin's experiments were conducted at very high speeds of rotation (about 20 percent of critical speed) and the accuracy of using the model to predict slower flows, for example, the rolling or slumping modes found in industrial kilns, is questionable. Additionally, the problem of quantifying the flow in the active layer for purposes of determining heat transfer cannot really be addressed by this methodology.

4.1 Flow of Granular Materials (Granular Flows)

The rapid deformation of bulk solids, such as sand, mineral ore, coal, grains, ceramic and metal powders, and so on, is termed granular flow. This definition covers the movement of materials in a wide array of mineral and materials processing applications including heat treatment, drying, cooling, ore reduction, and others. The description of the dynamic behavior of these materials involves aspects of traditional fluid mechanics, plasticity theory, soil mechanics, and rheology (Savage, 1989). Despite the fact that granular flow has been applied to the study of gravity flow in hoppers, rockfalls, snow avalanches, mudflows, and so forth in recent years, it has not found application in rotary kilns. However, it has long been recognized (Singh, 1978) that particle diffusion in rotary kilns proceeds by interparticle collision suggesting that granular flow behavior based on either the dilute or dense-phase kinetic theory might be a logical modeling step. Ferron and Singh (1991) showed experimentally that the magnitude of the axial diffusion coefficients lies between that of liquids and gases and

that the modeling of the axial flow goes beyond Seaman's equilibrium approach. They employed the dilute gas kinetic theory analogy to describe rotary kiln transport phenomena such as mass and heat transfer. Although similar models such as the dense gas theory were being explored at the same time in solving problems associated with chute flows, debris flow, and avalanches (Savage, 1989), the approach did not catch on for rotary kiln characterization.

The primary challenge in granular flow modeling is not in setting up the conservation equations for mass, momentum, and energy, but in establishing the stress/strain relationship for the particulate mass as this relationship depends on the flow regime and vice versa. Davies (1986) has compared the observed behavior of granular materials, subjected to shear stress, with other common types of flow behavior (Figure 4.1). The figure depicts the shear stress as a function of the dilation factor $\bar{\lambda}$ expressed as

$$\bar{\lambda} = \left(\frac{\nu^*}{\nu}\right)^{1/3} - 1 \tag{4.1}$$

Here, ν is the volume concentration of solids (or solids fraction) and ν^* is the corresponding value at the minimum possible void fraction that the material can maintain. For granular materials in a static condition, the particles fit together into a rigid grid. This means that some degree of stress can be sustained without inducing a flow. However, as the stress approaches some critical level, the particles begin to ride up on

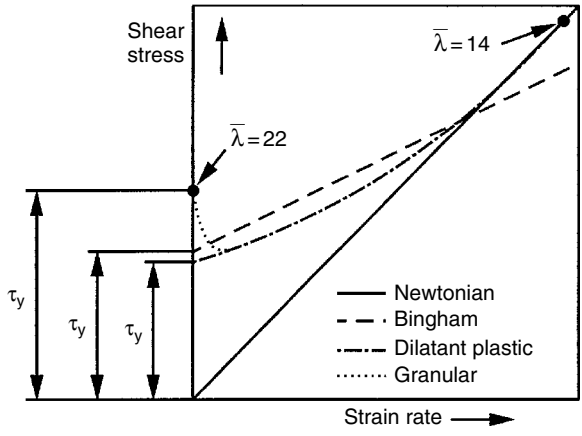

Figure 4.1 Comparison of granular flow behavior with other flow types (Davies, 1996).

one another and the grid commences dilation. At the critical stress, the dilation $\dot{\lambda}$ reaches a maximum and the material begins to flow. Once this occurs, the shear stress shows an incipient steep decline with increasing strain rate and it is this initial behavior that distinguishes granular flow from Bingham or dilatant plastic flow behaviors. Beyond a certain rate of strain the stress begins to increase again and the granular flow behaves like a dilatant plastic flow, that is, a nonlinear relationship between the shear stress and the rate of strain.

These fundamental aspects of the flow of granular material or bulk solids, similar to the flow in rotary kilns, have been reviewed by Savage (1979). Many theories have been considered in the effort to establish appropriate constitutive relations for such flows. As mentioned earlier, these theories extend from traditional soil mechanics to all types of viscous flows. The most important conclusions that can be drawn from these works to describe granular flow include the following:

1. Granular flow behavior extends beyond the critical state as defined by traditional soil mechanics literature. As a result of rapid deformation associated with the flow, inertia as well as shear-rate effects must be considered.
2. The dominant effect on the two-phase flow arises from particle-to-particle interactions whereas the interstitial fluid plays a minor role.
3. Because of particle-to-particle interaction, the transport processes are assumed to be governed by a field quantity called granular temperature, $\widetilde{T}$, which can be defined as the kinetic energy per unit mass contained in a random motion of particles.

It is therefore common to assume that the state variables that describe the rapid deformation response of granular materials would border on the parameters that describe the behavior of fluids and Coulomb type dissipation of energy (static). In view of the above it is common to find that the theories governing granular flow are formulated around the assumption of a continuum similar in some regard to viscous fluids; however, the equilibrium states of the theories are not states of hydrostatic pressure, as would be in the case of fluids, but are rather states that are specified by the Mohr-Coulomb criterion (Cowin, 1974). The advantage of continuum formulations over alternative particulate (stochastic) formulations is that use of continuum is more capable of generating predictive results. Mathematically one

can argue that any state variable, such as the solid fraction, ν, can only be either zero or unity depending upon whether a granule is present or not. By using the continuum approach it is common to represent ν by a continuous function of position so that its value might represent the average in the neighborhood of that position.

The mechanisms of momentum transfer (and hence stress generation) for granular flows include the following:

1. Static stresses resulting from the rubbing between particles (dry Coulomb type rubbing), which is independent of strain rate.
2. Translational stresses resulting from the movement of particles to regions having different velocity.
3. Collisional stresses resulting from inter-particle collision, which result in transfer of both momentum and kinetic energy.

The relative importance of these three mechanisms will depend on both the volume concentration of solids within the bed, that is, the dilatancy factor ($\overline{\lambda}$), and the rate of strain. The static contribution dominates at high particle concentration and low strain rates. In this situation the particles are in close contact and the shear stresses are of the quasi-static, rate independent Coulomb-type as described in soil mechanics literature (de Jong, 1964; Spencer, 1964; Mandl and Luque, 1970; and Roscoe, 1970). Conversely, at low particle concentrations and high strain rates, the mean free path of the particles is large compared with particle diameters and the interchange of particles between adjacent layers moving at different mean transport velocities may dominate stress generation. This situation is analogous to turbulent viscosity in fluid flow. At moderate particle concentration and high strain rate, collision between particles as against translation of particles to layers will dominate stress generation. This happens because there are rarely any void spaces of sufficient size for the interchange of particles over any significant distances. The case pertaining to low and moderate particle concentration was extensively studied by Bagnold (1954), a condition called the grain inertia regime where the dynamics of the actual particle collision become important. The applicable kinetic theories follow either hard sphere models, which assume that the interparticle collisions are instantaneous and therefore the collision trajectory is determined by the rules governing rigid body collisions (i.e., elastic, inelastic, etc.), or soft sphere models, which

assume that particle collisions are of finite duration. Both models have been used to describe the collisional interactions that give rise to the transport of momentum and kinetic energy in granular flows. In this grain inertia regime, the stress tensor is said to be strain rate dependent (Campbell and Gong, 1986), and might be expressed as,

$$\tau_{ij} \propto \left(d_{\mathrm{p}} \frac{du}{dy} \right)^2 \tag{4.2}$$

Equation (4.2) includes translational and collisional effects but not static effects. However, most engineering applications (e.g., chute flows) and other natural flow situations (mudflows, snow avalanches, debris flow, etc.) appear to fit into a regime for which the total stress must be represented by a linear combination of a rate-independent static component plus the rate-dependent viscous component just described (Savage, 1989). The flow patterns observed for material flow in rotary kilns appear to fit these descriptions and the constitutive equations for granular flow may apply within the relevant boundary conditions.

4.2 The Equations of Motion for Granular Flows

The equations of motion for granular flows have been derived by adopting the kinetic theory of dense gases. This approach involves a statistical-mechanical treatment of transport phenomena rather than the kinematic treatment more commonly employed to derive these relationships for fluids. The motivation for going to the formal approach (i.e., dense gas theory) is that the stress field consists of static, translational, and collisional components and the net effect of these can be better handled by statistical mechanics because of its capability for keeping track of collisional trajectories. However, when the static and collisional contributions are removed, the equations of motion derived from dense gas theory should (and do) reduce to the same form as the continuity and momentum equations derived using the traditional continuum fluid dynamics approach. In fact, the difference between the derivation of the granular flow equations by the kinetic approach described above and the conventional approach via the Navier Stokes equations is that, in the latter, the material properties, such as viscosity, are determined by experiment while in the former the fluid properties are mathematically deduced by statistical mechanics of interparticle collision.

Equations of motion and the pertinent constitutive equations for the flow of granular materials have been developed by Lun et al. (1984) using the hard sphere kinetic theory of dense gas approach. In this derivation a fixed control volume was considered in which a discrete number of smooth but inelastic particles are undergoing deformation. The resulting system of equations was given as follows:

1. Conservation of mass:

$$\frac{\partial \rho}{\partial t} = -\nabla \cdot (\rho \vec{u}) \tag{4.3}$$

   where $\vec{u}$ is the velocity of the bulk material, ρ (equal to $\nu\rho_p$) is the bulk density, and ν is the bulk solid fraction.

2. Conservation of momentum:

$$\rho \frac{du}{dt} = \rho \mathbf{b} - \nabla \cdot \mathbf{P} \tag{4.4}$$

   where **b** (a vector) is the body force, and **P** (a vector) is the total stress tensor which, unlike continuous fluid flow, comprises the three stress components mentioned earlier: (i) the static (frictional) stress P_f, (ii) the kinetic stress P_k that arises from the translation (or streaming) of particles, and (iii) the stresses resulting from particle collisions P_c. It is perhaps worth pointing out that the translational stress P_k is analogous to the Reynolds stresses for turbulent flow of fluids.

In addition to mass conservation, Equation (4.3), and momentum conservation, Equation (4.4), a third relationship that is required to describe the flow is some form of energy conservation equation. The total energy per unit mass of the granular material, E, may be broken into three components (Johnson and Jackson, 1987):

1. The kinetic energy, E_k, associated with the local average velocity u

$$E_k = \frac{1}{2}|u|^2 \tag{4.5}$$

2. The pseudo-thermal energy, E_{PT}, associated with deviations of the motion of individual particles from the local average; E_{PT} can be represented by the kinetic energy definition of temperature as

$$E_{PT} = \frac{1}{2}C^2 = \frac{3}{2}\tilde{T} \tag{4.6}$$

where c is the local velocity; $C = c - u$ is called the peculiar velocity. C^2 is the mean square of the velocity fluctuations about the mean. $\widetilde{T}$ in Equation (4.6) is the kinetic theory definition of temperature called granular temperature (Johnson and Jackson, 1987) or grain temperature (Lun et al., 1984) which was defined earlier as the kinetic energy per unit mass contained in the random motion of particles (Zhang and Campbell, 1992). This must not be confused with the sensible heat or the true thermal internal energy of the solid material, that is, the enthalpy that might be required for heat transfer rather than momentum transfer. The total kinetic energy flux q will therefore be composed of the sensible heat flux q_{h}, and the flux of the pseudo-thermal energy, q_{PT}. The former is related to the thermodynamic temperature gradient and the effective thermal conductivity of the assembly of solid particles, while the latter is related to the gradient in the kinetic theory definition of temperature, that is, the granular temperature or grain temperature.

The conservation equation for the true thermal energy (sensible heat) is now distinguished as

$$\rho \frac{\mathrm{D}E_{\mathrm{h}}}{\mathrm{D}t} = -\nabla \cdot q_{\mathrm{h}} - P_{\mathrm{f}} : \nabla \boldsymbol{u} + \gamma \tag{4.7}$$

where $\mathrm{D}/\mathrm{D}t$ is the material derivative. $P_{\mathrm{f}} : \nabla u$ represents the rate of working of the frictional component of the stress tensor, while γ is the rate of dissipation due to the inelasticity of collisions between particles. In Equation (4.7), it is implied that work done by the frictional component of the stress tensor is translated directly into sensible heat and does not contribute to the pseudo-thermal energy (granular temperature) of the particles. It is worth mentioning that Equation (4.7) is the energy equation for the sensible heat or the true thermal energy transport and, since it does not influence the granular flow, is usually treated separately. In addition, the magnitude of the last two terms in Equation (4.7) (i.e., dissipation of frictional energy) is small compared with the thermal (thermodynamic) energy contribution to energy intensive process devices such as rotary kiln and may therefore be neglected during heat transfer calculations. Hence the conservation of kinetic energy in the absence of the terms that do not influence the flow field might be given as (Johnson and Jackson, 1987; Ahn et al., 1991; etc.):

$$\frac{3}{2}\rho \frac{\mathrm{D}\widetilde{T}}{\mathrm{D}t} = -\nabla \cdot q_{\mathrm{PT}} - (P_{\mathrm{k}} + P_{\mathrm{c}}) : \nabla \boldsymbol{u} - \gamma \tag{4.8}$$

In order to solve for the foregoing conservation equations to establish the granular flow field they must be closed by plausible constitutive relations for the stress terms, P_k, P_c, and P_f, the kinetic energy flux, q, and rate of dissipation by inelastic collision, γ, along with suitable boundary conditions. Applying these equations to describe the flow of material in the transverse plane of the rotary kiln will require a true quantification of the actual flow properties, for example velocity, in the various modes of rotary kiln observed and described earlier in Chapter 2.

4.3 Particulate Flow Behavior in Rotary Kilns

The rotary kiln is oftentimes considered to be a black box into which materials are fed at one end and discharged at the other without knowledge of what happens with the flow behavior in between. It has therefore been a great research curiosity to observe the flow patterns at the various zones through experiments. But, unlike gas flow, which can be visualized on a full scale setup, most particulate flow experiments can only be observed through an end piece. Nevertheless, they have successfully provided adequate information for flow modeling. Recent noninvasive measurement techniques such as use of NMR (Nakagawa et al., 1993), positron emission particle tracking (Parker et al., 1997), and photonic sensors (Hsiau and Hunt, 1993; Boateng and Barr, 1997) have provided sufficient evidence and boundary conditions for flow modeling.

Using photonic sensors, and a 1 m rotary drum Boateng (1993) characterized the flow behavior of high-density spherical polyethylene particles (elastic material), non-spherical long grain rice (inelastic material), and irregular limestone particles (industrial material). Visual observations were made with regard to the slipping, slumping, rolling, and cataracting as previously observed (Henein et al., 1983a). Henein et al. had experimentally studied bed behavior diagrams and identified various types of bed motion. Boateng and Barr (1997) successfully quantified active layer thickness, bed expansion, and dynamic angle of repose within a wide range of the operational variables. The active layer was quantified in terms of its shape, symmetry, and depth. Dilation within the active layer was quantified by determining the solid fraction there and comparing it with the plug flow region. In analyzing the flow behavior some of the key parameters that characterize

rheological behavior of granular solids, specifically the velocity parallel to the bed surface, the granular temperature, the solid fraction, and the active layer depth, were computed. One objective of the exercise was to compare the similarities between the rapidly flowing active layer and other granular flow systems so as to establish and justify the use of the constitutive equations developed for granular flow in kilns. This was accomplished by estimating the mean value of the velocity from instantaneous velocities of particles flowing past an optical fiber probe unit, and the variance of the velocity fluctuation with which the granular temperature, $\widetilde{T}$ could be computed. Other granular flow parameters including the solid fraction in the transverse plane, also known as the solids linear concentration in the direction of the flow (Ahn et al., 1991), could be measured. Also calculated was the mean shear rate $\Delta u/\delta$ where Δu was the local velocity difference between the surface and the active layer/plug flow interface and δ is the local active layer depth normal to the surface plane. An overview of the experimental results is discussed herein (Boateng and Barr, 1997).

4.4 Overview of the Observed Flow Behavior in a Rotary Drum

The flow behavior patterns of polyethylene particles at various percent fills (i.e., 3.3, 8.5, 15, and 29 percent) and operated at drum speeds ranging between 1 and 5 rpm and also for rice grains loaded at 3.3, 8.5, and 10 percent fills and operated from 3 through 5 rpm have been discussed in published works including Boateng and Barr (1997). The results show that the surface velocity profile is parabolic (Figure 4.2) indicating that particles accelerate rapidly from the apex (top corner with maximum potential energy) up to a location around the mid-chord and then decelerate. The deceleration is a result of the impact of the rotating wall on the material at the base, as would be expected in a confined flow. The mid-chord velocity could be observed to be as high as 110 cm/s, about seven times the circumferential velocity of the drum wall, and an indication of a very rapid flow of particles over the exposed bed surface.

The parabolic nature of the surface velocity is consistent with observations made by Singh (1978) who also used similar polyethylene pellets in a rotary kiln experiment. One observation about the free surface flow is that the symmetry in the velocity profile is quick to

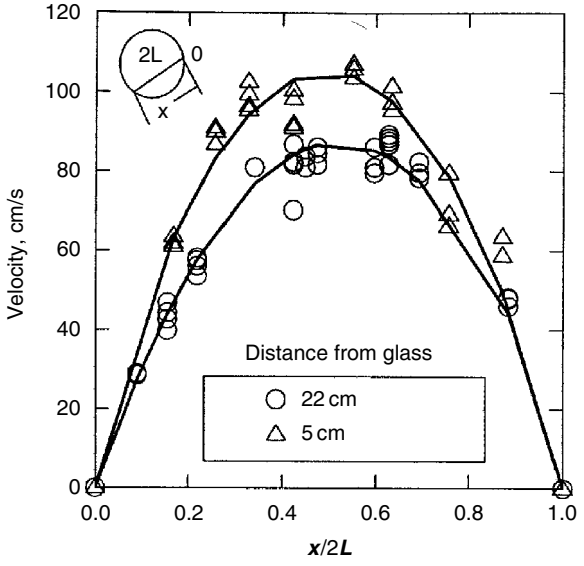

Figure 4.2 Measured exposed surface velocity profile in the active layer (15 percent fill and 5 rpm).

disappear with particle inelasticity and operational conditions. Hence velocity profiles can be symmetric or asymmetric due to variations in bed depth (or percent fill) and drum speed. For irregular and inelastic materials, a considerable amount of energy is required for the particles to rearrange themselves and in doing so pile up at the apex in order to minimize energy. This potential energy buildup is subsequently released very rapidly in a manner similar to an avalanche. For inelastic industrial materials such as limestone, bifurcations in the velocity profiles are quickly developed at the free surface. With regard to the active layer depth several works have reported qualitative characterization of it but Boateng (1993) was first to quantify it. For example Henein et al. (1983a) reported the thickness of the active layer for relatively deep beds to be about 10 percent of the bed depth at mid-chord. However, with the help of optical fiber probes Boateng (1993) showed that 10 percent is not always the case but, rather, depends on the material. Measurements with polyethylene pellets as the bed material showed the thickness of the active layer could be as high as 30 percent of the bed depth at mid-chord (Figure 4.3). However, active layer depths for most inelastic materials are generally less. Hence the extent of the active layer thickness can be expected to

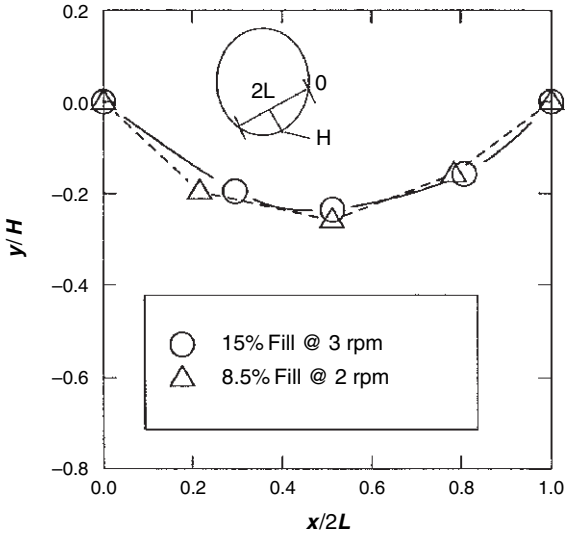

Figure 4.3 The shape and depth of active layer at mid-chord.

depend on the physical properties of the material that determine the ability of the granular material to shear under stress. Nonintrusive measurements that have recently appeared have substantiated these findings (Parker et al., 1997).

Analysis of the velocity profile as a function of depth shows some agreement with inclined chute flow experiments with polyethylene pellets (Savage, 1979). The behavior can be characterized as typical of flows over rough surfaces depicting drag flows that are mathematically classified as tractrix (from Latin tractum). Except for the regions near the free surface, a constant shear rate ($du/dy = const$) is deduced implying a uniform simple shear flow (Figure 4.4). Measurement of the granular temperature, the velocity fluctuation, and the linear concentration could similarly be made (Figures 4.5 and 4.6).

Like its counterpart in the kinetic theory of dense gases, that is, thermodynamic temperature, granular temperature can either conduct away from the free surface into the bed or vice versa. The profile shown here indicates that there can be a granular temperature gradient between the bed surface and the bulk bed in agreement with the computer simulation of Zhang and Campbell (1992) for couette flow of granules. It is observed that the granular temperature is high in the regions where there is a mean velocity gradient and therefore it is not surprising to see granular conduction into the bed burden. An

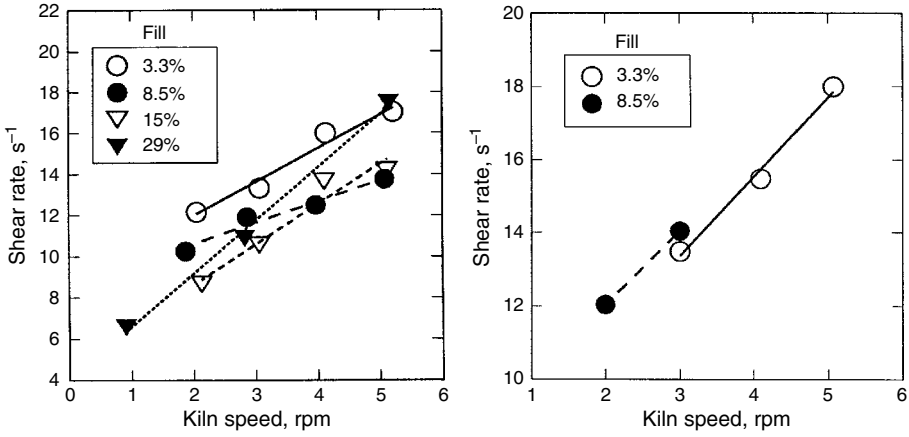

Figure 4.4 Shear rate, du/dy, at active layer. Left: polyethylene pellets; right: limestone.

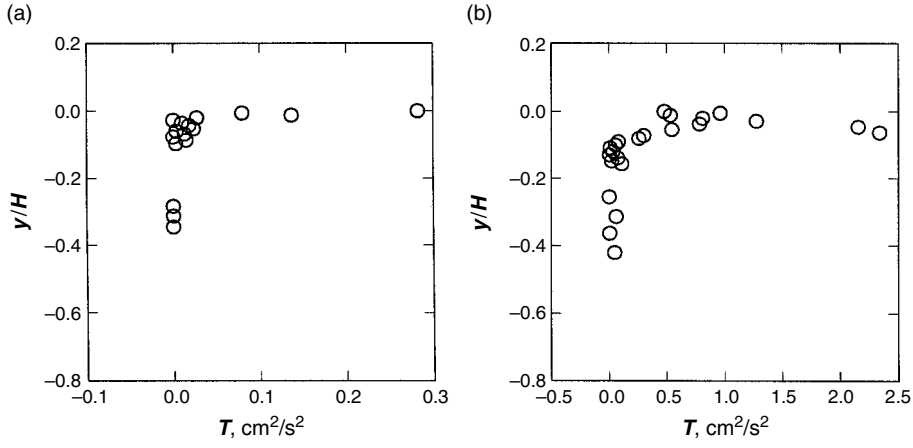

Figure 4.5 Measured granular temperature for the active layer for polyethylene pellets at 29 percent fill: (a) 1 rpm; (b) 3 rpm.

increase in the drum speed from 1 to 3 rpm results in an order of magnitude increase in the granular temperature. The profile for the linear concentration (Figure 4.6) shows that there is also a gradient between the surface and the bulk bed. Material dilation in the direction normal to the bed surface is not very significant according to visual observations through the glass end piece. This is not surprising for rolling bed behavior; material balance calculations have shown that bed expansion in the normal direction does not exceed 5 percent.

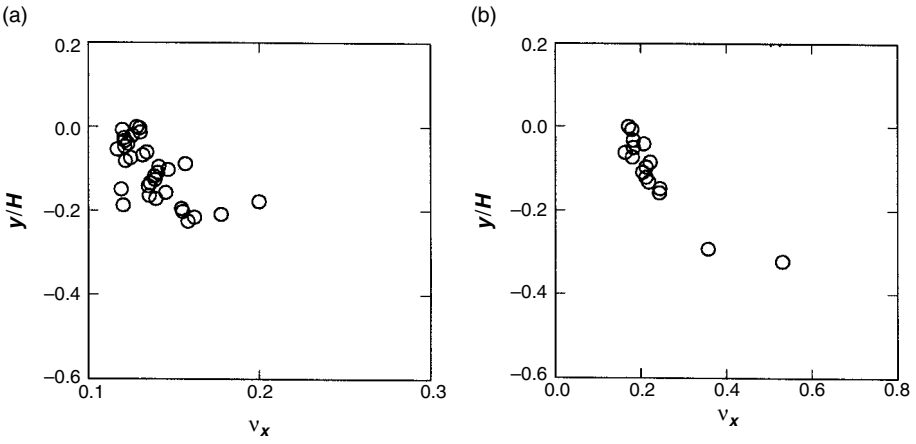

Figure 4.6 Measured linear concentration profile in the active layer for polyethylene pellets: (a) 15 percent fill and 3 rpm; (b) 29 percent fill at 5 rpm.

4.4.1 Modeling the Granular Flow in the Transverse Plane

The flow behavior described can be modeled in several ways including the use of the kinetic theory approach employed for avalanche and debris flow. Ferron and Singh (1991) were first to apply such theory to describe the observations in a rotary kiln using the dilute phase kinetic theory. However, the experimental work described herein (Boateng and Barr, 1997) suggests that dense phase kinetic theory might be most suitable. The model described here employs the dense phase kinetic theory constitutive equations developed for elastic or slightly inelastic granular materials and applied to the boundary conditions of the rotary drum. Following the experimental observations and measurements described (Boateng and Barr, 1997) plausible solutions are found by exploring the boundary layer flow similarities with the rolling bed active layer flow.

4.5 Particulate Flow Model in Rotary Kilns

Plausible arguments can be made about the similarities of the active layer flow and flows of isotropic fluid over flat plates. Additionally, previous works on granular flow on inclined planes (e.g., chute flow)

suggest that the constitutive equations derived for rapidly shearing (slightly inelastic) granular material and based on the analogy of kinetic theory of dense gases (Lun et al., 1984) are adequate in interpreting the experimental results. Although other theories exist, for example, plastic formulations (Mandl and Luque, 1970), they have not been widely tested for rapidly shearing granular flows.

4.5.1 Model Description

The domain for which a solution to the flow problem is sought is depicted in Figure 4.7. As shown in the figure, two distinct regions, (i) the non-shearing (plug flow) region, and (ii) the shearing region that forms the active layer near the bed surface, can be discerned by an interfacial boundary which is a few particles away from the zero velocity line. At this boundary, particles are sustained by the dynamic angle of repose. In the plug flow region the particles rotate with the kiln as a rigid body and the strain rate in this region is zero. The flow of particles within the active layer near the upper bed surface is rather more complex since it involves all the aspects of granular flow discussed earlier. In this region the material can acquire any of

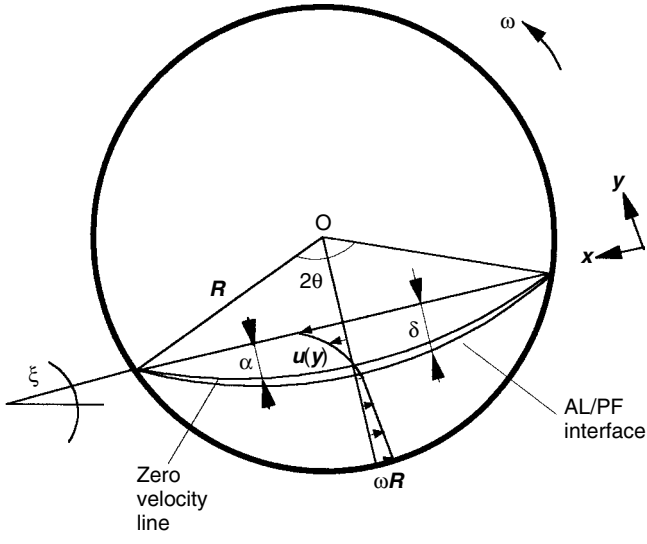

Figure 4.7 Granular flow calculation domain.

the several modes described earlier, such as slumping, which is a slow flow occurring when the bed inclination just exceeds the static angle of repose of the material; rolling bed, for which the material is continuously sheared and the flow, as well as diffusion, is the result of interparticle collisions. To model the flow in the cross section we will focus on the rolling mode behavior because of its importance to industrial kiln operation then later discuss the mode-to-mode transition regimes using the rolling bed results. For the rolling mode the plug flow region might be anticipated to behave as a rigid lattice of particles rotating with the kiln wall without slippage. The velocity within the plug flow region is a linear function of radius. Hence a solution for the flow field is therefore required only for the active layer near the upper surface of the bed. However, the location of the interface between this region and the active layer is not known *a priori* and the model must allow prediction of its location.

4.5.2 Simplifying Assumptions

The primary assumptions for modeling granularity in the transverse plane of a rotating cylinder are as follows:

1. The bed material consists of cohesionless particles that possess a relatively high coefficient of restitution. This assumption places important emphasis on the role of interparticle collision on momentum transfer and permits the use of the equations of Lun et al. (1984).
2. Particles are spherical, rigid, and slightly inelastic, such as the polyethylene pellets used in the experimental work.
3. The bed motion is in the rolling mode and the active layer is considered to be thin relative to the bed depth (the ratio of the active layer depth at mid-chord to the chord length was less than 0.04 in the experiments). The granular temperature in the active layer is assumed constant in the radial direction at each bed surface position.
4. The motion is essentially two-dimensional in the transverse plane since the transverse velocity is several orders of magnitude greater than the axial velocity. Also particle flux into the active layer at the right quadrant is assumed to equal the particle flux into the plug flow

region at the left quadrant (symmetry) and therefore only half of the two-dimensional domain is considered.

5. The particle ensemble behaves as a continuum and the flow properties, for example, solids concentration, are assumed to be continuous functions of position.

4.5.3 Governing Equations for Momentum Conservation

The governing equations for the flow field are similar to those derived for conventional fluids, for example the Navier Stokes equations for Newtonian isotropic material. However, in the latter case, flow properties such as viscosity are experimentally determined. For the case of the dense gas theory and, by extension, granular flows, collisions between particles play a significant role in the exchange of both energy and momentum. Under these conditions kinetic energy conservation must also be considered in the formulation along with momentum and mass transport. The governing equations (Equations 4.3–4.6) can be restated as (Lun et al., 1984)

$$\frac{\partial \rho}{\partial t} + \nabla \cdot (\rho u) = 0 \tag{4.9}$$

$$\rho \frac{Du}{Dt} = \rho g - \nabla \cdot \mathbf{P} \tag{4.10}$$

$$\frac{3}{2}\rho \frac{D\widetilde{T}}{Dt} = -\nabla \cdot q_{\mathrm{PT}} - \mathbf{P} : \nabla u - \gamma \tag{4.11}$$

where u is the bulk velocity, $\rho = \nu\rho_{\mathrm{p}}$ is the bulk density and ν is the solids volume fraction. $\mathbf{P}$ is the total stress tensor, which consists of both static and kinetic (streaming and collision) components. The term q_{PT} is the flux of pseudo-thermal energy defined by the kinetic energy definition of temperature, $\widetilde{T}$, also known as granular temperature (Johnson and Jackson, 1987), while γ is the dissipation of pseudo-thermal energy due to inelastic collision of particles. The kinetic contribution of the stress tensor might be given as (Lun et al., 1984)

$$P = \left[\rho\widetilde{T}(1 + 4\eta\nu g_0) - \eta\mu_{\mathrm{b}}\nabla \cdot u\right] I - \left\{\frac{2\mu}{\eta(2-\eta)g_0}\left(1 + \frac{8}{5}\eta\nu g_0\right)\left[1 + \frac{8}{5}\eta(3\eta - 2)\nu g_0\right] + \frac{6}{5}\mu_{\mathrm{b}}\eta\right\} S \tag{4.12}$$

derived by considering the pair distribution function in collision theory. In Equation 4.12, S is the deviatoric stress which is given by,

$$S = \frac{1}{2}\left(u_{i,j} + u_{j,i}\right) - \frac{1}{3}u_{k,j}\delta_{ij} \tag{4.13}$$

where δ_{ij} is the kronecker delta; that is, $\delta_{ij} = 1$ for $i = j$, and $\delta_{ij} = 0$ for $i \neq j$.

The flux of pseudo-thermal energy is expressed as (Johnson and Jackson, 1987)

$$\begin{aligned} q_{\mathrm{PT}} = &- \frac{\lambda_i}{g_0}\left\{\left(1 + \frac{12}{5}\eta\nu g_0\right)\left[1 + \frac{12}{5}\eta^2(4\eta - 3)\,\nu g_0\right]\right. \\ &\left. + \frac{64}{25\pi}(41 - 33\eta)(\eta\nu g_0)^2\right\}\nabla\widetilde{T} \\ &- \frac{\lambda_i}{g_0}\left(1 + \frac{12}{5}\eta\nu g_0\right)\frac{12}{5}\eta(2\eta - 1)(\eta - 1)\frac{d}{d\nu}\left(\nu^2 g_0\right)\frac{\widetilde{T}}{\nu}\nabla\nu \end{aligned} \tag{4.14}$$

The dissipation of energy due to inelastic collisions may be written as (Johnson and Jackson, 1987)

$$\gamma = \frac{48}{\sqrt{\pi}}\eta(1 - \eta)\rho_{\mathrm{p}}\frac{\nu^2}{d_{\mathrm{p}}}\widetilde{T}^{3/2} \tag{4.15}$$

The nomenclature is consistent with existing granular flow literature (Lun et al., 1984; Johnson and Jackson, 1987; Natarajan and Hunt, 1998) but key parameters in these constitutive equations can be defined using the analogy of fluid flow as follows:

μ_{b} [$= 256\mu\nu^2 g_0/5\pi$] bulk viscosity for perfectly elastic particles; $\eta\mu_{\mathrm{b}}$ is the bulk viscosity for inelastic particles;

λ [$= 75m\sqrt{\widetilde{T}/\pi}/64d_{\mathrm{p}}^2$] is the granular conductivity;

λ_i [$= 8\lambda/\eta(41 - 33\eta)$] is the granular conductivity for inelastic particles;

η [$= 1/2(1 + e_{\mathrm{p}})$] is the average value between the coefficient of restitution of the particle, e_{p}, and that of a perfectly elastic particle, $e_{\mathrm{p}} = 1$.

μ [$= 5m\sqrt{\widetilde{T}/\pi}/16d_{\mathrm{p}}^2$] is the shear viscosity, where m and d_{p} are particle mass and diameter, respectively;

μ_i $[= \mu/\eta(2-\eta)]$ is the shear viscosity for inelastic particles;

g_0 $[= 1/(1-\nu/\nu^*)^{1/3}]$ is a radial distribution function at contact during binary collusion or the dilation factor. In this term ν^* is the maximum shearable solids volume fraction.

The reason for assuming that the active layer is thin relative to the bed depth is to confine the domain for which a solution to the flow problem is sought to the active layer, thus avoiding the computational demands of solving for the already-known velocities in the plug flow region. The obvious task is to develop approximate solutions analogous to those of other thin flows, in other words, of boundary layer flows. To do so it is necessary to normalize the governing equations according to the dimensions of the kiln cross section and establish whether these equations can be reduced to parabolic equations similar to those for flow over a flat plate as suggested earlier. Recasting Equations (4.9–4.12) into primitive variables yields the steady-state continuity, momentum, and kinetic energy equations:

$$\frac{\partial u}{\partial x} + \frac{\partial v}{\partial y} = 0 \tag{4.16}$$

$$\rho\left[u\frac{\partial u}{\partial x} + v\frac{\partial u}{\partial y}\right] = \rho g \sin\xi - \frac{\partial P_{xx}}{\partial x} - \frac{\partial P_{xy}}{\partial y} \tag{4.17}$$

$$\rho\left[u\frac{\partial v}{\partial x} + v\frac{\partial v}{\partial y}\right] = -\rho g \cos\xi - \frac{\partial P_{xy}}{\partial x} - \frac{\partial P_{yy}}{\partial y} \tag{4.18}$$

$$\rho\left[u\frac{\partial \tilde{T}}{\partial x} + v\frac{\partial \tilde{T}}{\partial y}\right] = -\left[\frac{\partial q}{\partial x} + \frac{\partial q}{\partial y}\right] - \left[P_{xx}\frac{\partial u}{\partial x} + P_{xy}\frac{\partial v}{\partial x} + P_{yx}\frac{\partial u}{\partial y} + P_{yy}\frac{\partial v}{\partial y}\right] - \gamma \tag{4.19}$$

We can now invoke the simplifications derived from the thin flow assumption to solve for the velocity distribution in the active layer. This requires some normalization using Δ and H (Figure 4.8).

The coordinates appropriate to the active layer may be defined in cartesian coordinates with field variables taken with respect to x and y where, from assumption (iv), $-L \le x \le L$ and $0 \le y \le -H$. These variables are Δ, the depth of the active layer at mid-chord of the free surface plane, and L, half of the mid-chord length. If the angle subtended by the boundary interface is the dynamic angle of repose, ξ, then $\tan\xi$ is the coefficient of dynamic friction and the stresses can be normalized with the gravity term as (Savage and Hutter, 1989)

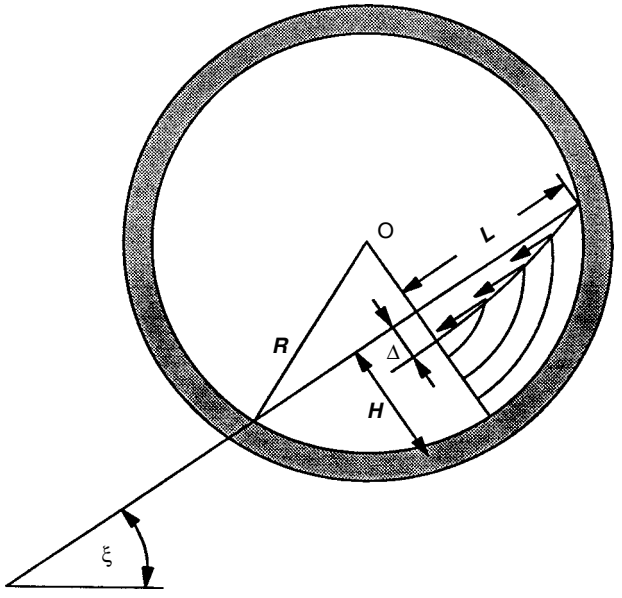

Figure 4.8 Variables employed in the normalization of granular flow equations.

$$(x, y) \rightarrow ([L]x^*, [\Delta]y^*)$$
$$(u, v) \rightarrow \left([(gL)^{1/2}]u^*, [\Delta/L(gL)^{1/2}]v^*\right) \tag{4.20}$$
$$(P_{xx}, P_{yy}, P_{xy}) \rightarrow [\rho g \cos\xi\Delta](P^*_{xx}, P^*_{yy}, \tan\xi P^*_{xy})$$

For a detailed derivation, interested readers are referred to the pertinent literature (Boateng, 1998). As $\Delta/L \rightarrow 0$ the equations reduce to boundary layer equations which, deleting the * from the non-dimensional terms has the form

$$\frac{\partial u}{\partial x} + \frac{\partial v}{\partial y} = 0 \tag{4.21}$$

$$u\frac{\partial u}{\partial x} + v\frac{\partial v}{\partial y} = \sin\xi - \sin\xi\frac{\partial P_{xy}}{\partial y} \tag{4.22}$$

For this thin flow, the y-wise momentum equation becomes the overburden pressure

$$\frac{\partial P_{yy}}{\partial y} = 1, \quad \text{and} \quad P_{yy} = \int_0^{\Delta} v\,dy \tag{4.23}$$

It should be noted that, so far as nothing is said about the stresses, which depend on the boundary conditions, Equations (4.21) and (4.22) are similar to those derived for flow over a flat plate (Schlichting, 1979). To solve for these equations the continuity equation can be rearranged as

$$v = -\int_0^y \left(\frac{\partial u}{\partial x}\right) \mathrm{d}y \tag{4.24}$$

Substituting Equation (4.24) into the corresponding momentum equation, an approximate solution similar to that obtained by von Karman for flow over a flat plate can be sought (Schlichting, 1979). Having demonstrated the similarity between the active layer flow and boundary layer flow equations, one convenient solution approach is to recast them into momentum integral equations and find simple solutions by integration over the appropriate control volume. Such an exercise provides additional highlights of the physical interpretation of the complex granular flow equations as applied to the rotary kiln cross section. It will also allow the use of some of the experimentally measured parameters for boundary conditions to the specific flow problem.

4.5.4 Integral Equation for Momentum Conservation

So far the problem has been dealt with by stating the continuum equations for material flow and these equations have been reduced to parabolic equations involving unknown stresses by using the geometry of a rolling bed. It can now be shown that, if the flow behaves as a continuum, then the same equations can be deduced by simply considering material and momentum balance over a control volume in the active layer of the bed (Figure 4.9).

By proceeding in a manner similar to that employed in deriving the von Karman equation for a developing boundary layer, the system of partial differential equations (Equations 4.21 and 4.22) can be reduced to the ordinary differential equation

$$\rho \frac{\mathrm{d}}{\mathrm{d}x}\left(\int_0^H \left(u^2 - u_\delta u\right) \mathrm{d}y\right) \mathrm{d}x + \frac{\mathrm{d}u_\delta}{\mathrm{d}x}\left(\int_0^H \rho u \mathrm{d}y\right) \mathrm{d}x = \sum F_x \tag{4.25}$$

It can be readily shown that Equation (4.25) can also be obtained by substituting Equation (4.24) into the continuity and momentum equations directly and integrating by parts. It should be emphasized that, provided no statement is made about the stresses or the net

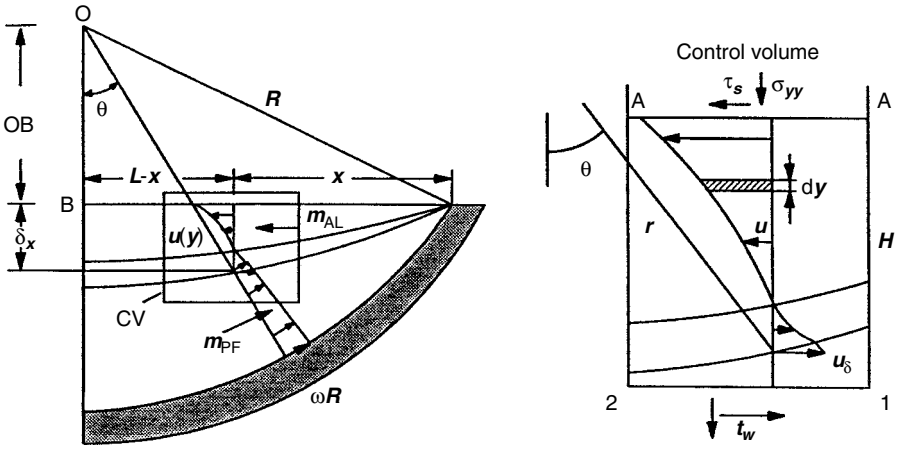

Figure 4.9 Control volume for deriving integro-momentum equations.

forces acting on the control volume, the net momentum equation is the same as that governing fluid flow, otherwise known as the Blasius problem (Schlichting, 1979). In Equation (4.25), u_δ, the velocity at the transition from the active layer to the plug flow, is a function of radius only ($u_\delta = \omega r$) but the radius for this transition requires knowledge of the active layer depth, δ_x, at that distance, x, from the apex. From the geometry in Figure 4.9 it can be shown that

$$r^2 = (L - x)^2 + (\mathrm{OB} + \delta_x)^2 \tag{4.26}$$

$$\cos\theta = \frac{(\mathrm{OB} + \delta_x)}{r} \tag{4.27}$$

where OB is the distance from the kiln's centerline to the bed surface. These geometric relationships will introduce nonlinearities in Equation (4.25) and an iteration procedure would be required in order to solve for the active layer depth. Having now derived the momentum conservation (Equation 4.25) in the active layer the next step is to proceed with the evaluation of the force terms. The forces acting on the control volume (Figure 4.10) include the body force and the forces that are generated by the stresses described earlier. The net force is equal to

$$-\tau_w - \mathrm{d}x + \sigma_N \mathrm{d}x + \rho g \mathrm{d}x \tag{4.28}$$

where σ_N is the overburden pressure and is given as

$$\sigma_N = P_{yy} + P_{xx} \tag{4.29}$$

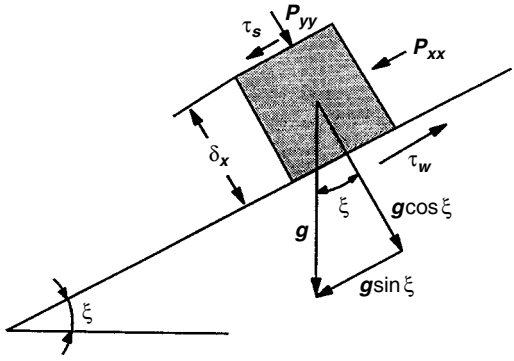

Figure 4.10 Force (pressure) distribution on control volume.

The top face of the control volume can be considered the free surface and therefore the shear stress is zero (plane A-A in Figure 4.9). The normal stress at this surface is due to the forces exerted by the freeboard gas. If there is no significant saltation of particles on the free surface, then the normal stress at this plane is also zero and equating the net momentum to the net force yields the integral momentum equation

$$\rho\frac{\mathrm{d}}{\mathrm{d}x}\left(\int_0^{\delta}\left(u^2 - u_{\delta}u\right)\mathrm{d}y\right) + \frac{\mathrm{d}u_{\delta}}{\mathrm{d}x}\int_0^{\delta}\rho u\mathrm{d}x = -\tau_w + P_{xx}\mathrm{d}y + \rho g\sin\xi \quad (4.30)$$

The second term on the left of Equation (4.30) would, in fluid flow, be equal to the hydrostatic pressure according to Bernoulli's equation. For granular flow on an incline this term is equivalent to the driving force parallel to the inclined plane and hence may be equated to the overburden pressure in the *x*-direction, that is,

$$\frac{\mathrm{d}u_{\delta}}{\mathrm{d}x}\int_0^{\delta}\rho u\mathrm{d}y = P_{xx} \quad (4.31)$$

Assembling the results obtained thus far yields the expression

$$\rho\frac{\mathrm{d}}{\mathrm{d}x}\left(\int_0^{\delta}\left(u^2 - u_{\delta}u\right)\mathrm{d}y\right) = \rho g\sin\xi - \tau_w \quad (4.32)$$

The final task before proceeding with its solution is to derive an appropriate expression for the shear stress acting over the bottom surface of the control volume, τ_w.

The shear stress is a combination of contributions from static and kinetic stresses. The extent of each contribution might be determined by the operational parameters, that is, the rotational speed, degree of

fill, and so on. The various modes of bed behavior can therefore be related to the stresses acting on the material within the depth of the active layer. These modes can be mathematically described as follows:

1. Slumping bed: When the rotation and/or collision of particles are constrained and if $\partial u/\partial y > 0$ then the shear stress is static and is simply given as

$$\tau_w = \rho g \cos\xi \tan\phi \tag{4.33}$$

where ϕ is the static angle of repose. This situation occurs for slumping bed behavior where there is no interparticle collision contribution to the shearing of the active layer (Henein et al., 1983b). The corresponding momentum equation is

$$\rho \frac{d}{dx}\left(\int_0^{\delta} (u^2 - u_\delta u)\, dy\right) = \rho g \sin\xi - \rho g \cos\xi \tan\phi$$
$$= g \cos\xi (\tan\xi - \tan\phi) \tag{4.34}$$

As Equation (4.34) indicates, if $\xi > \phi$, the flow is accelerated, while, if $\xi < \phi$, the flow is damped. When $\xi = \phi$, it can be said that the flow is indeterminate (Kanatani, 1979). Suffice it to say that damped flow is the mode for slipping bed behavior.

2. Rolling Bed: From the flow experiments discussed earlier, it can be said that the rolling bed is the situation where the kinetic stress is the driving force for material flow, that is, when the bed is in the rolling mode the material in the active layer is in a continuous shearing mode. In this case all the aspects of granular flow come into play and the shear stress is deduced from the constitutive equations we have described earlier. Many forms of the shear stress expressions exist in the literature, however, they are all variants of the equation first proposed by Bagnold (1954), which is given as

$$\tau_w = - c_i \rho_p \left(d_p \frac{du}{dy}\right)^2 \tag{4.35}$$

where c_i is Bagnold's constant (Campbell and Gong, 1986). We can now employ the stress/strain rate relationship from the constitutive equations derived through the analogy of kinetic theory of dense gases (Lun et al., 1984), that is,

$$\tau_w = C' \frac{du}{dy} \tag{4.36}$$

where the apparent viscosity, C', is a function of the dilation, $C' = f(\rho_p; d_p; e_p; \nu; \widetilde{T})$ and is related to the properties of the bed (Appendix 4A)

$$C' = -\rho_p d_p g_2(\nu)\widetilde{T}^{1/2} \tag{4.37}$$

where $g_2(\nu)$ is a term relating the viscosity to flow properties such as the coefficient of restitution of the particles, $\eta\{= (1/e_p)/2\}$, the solids fraction, ν, and is derived in Appendix 4A as

$$g_2(\nu) = \frac{5\sqrt{\pi}}{96}\left[\frac{1}{\eta(2-\eta)g_0} + \frac{8}{5}(3\eta-1)\frac{\nu}{(2-\eta)} + \frac{64}{25}\left\{\frac{\eta(3\eta-1)}{(2-\eta)} + \frac{12}{\pi}\right\}\nu^2 g_0\right] \tag{4.38}$$

Inserting this result for the shear stress in Equation 4.32 the momentum conservation equation takes on its final form:

$$\frac{d}{dx}\rho\int_0^{\delta}(u^2 - u_\delta u)dy = \rho g \sin\xi + g_2(\nu)\rho_p d_p \widetilde{T}^{1/2}\frac{du}{dy} \tag{4.39}$$

We notice that this equation involves the shear rate, dy/dy, in the active layer, the particle dilation of the bed, the granular temperature, and gravity, all of which are granular flow characteristics that were previously discussed under experimental overview. The equation points to the fact that boundary layer analogy can be combined with the constitutive equations of Lun et al. (1984) to arrive at a single analytical model which can be used to predict the depth and velocity of the active layer. It should be mentioned that although the kinetic energy equation has been avoided in the derivation of the momentum equations, its solution is required in order to obtain the granular temperature for Equation (4.39). As will soon be shown, in this particular case, a corrector-predictor numerical technique may be used to estimate $\widetilde{T}$ to simplify the calculations.

4.5.5 Solution of the Momentum Equation in the Active Layer of the Bed

Equations (4.34) and (4.39) represent the integro-differential equations for the bulk material flow in the bed active layer. However, in order to proceed further a suitable form for the velocity profile is required.

In choosing this suitable velocity function, it is necessary to account for the boundary conditions (i) at the free surface, and (ii) at the interface between the active and the plug flow region of the bed; and also to satisfy the requirement of continuity at the point where the solution in the active layer is joined to the plug flow solution. However, it is necessary to first consider the material balance for the bed section being considered. The material balance at an arbitrary x-position in the free surface plane establishes $\dot{m}_{AL} = \dot{m}_{PF}$ (Figure 4.11) or stated mathematically,

$$\rho_{AL} \int_0^{\delta_x} u_{AL}(x, y)\, dy = \rho_{PF} \int_{r_x}^{R} u_{PF}(r) dr \tag{4.40}$$

Recognizing that the bulk density is simply the particle density times the solid fraction ($\rho = \rho_p \nu$), and that, within the plug flow region $u = \omega r$, this equation simplifies to (dropping the subscript AL for velocity in the active layer)

$$\nu_{AL} \int_0^{\delta} u dy = \nu_{PF} \int_{r_x}^{R} \omega r\, dr \tag{4.41}$$

which, after integration of the right-hand side, gives

$$\nu_{AL} \int_0^{\delta} u dy = 0.5 \nu_{PF} \omega \left[R^2 - \left(\frac{H + \delta_x}{\cos\theta} \right)^2 \right] \tag{4.42}$$

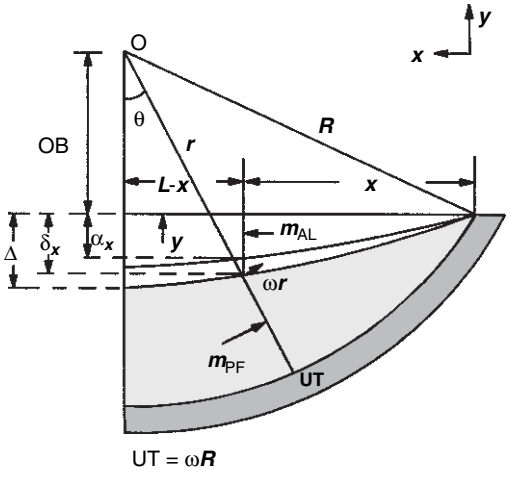

Figure 4.11 Material balance between active layer and plug flow region.

In Equation (4.42) $u = u_{AL}(x, y) = f(y)$ is the active layer velocity function which includes the actual active layer depth. At mid-chord, the global material balance for the entire cross section is satisfied and since the subtended angle there (i.e., θ) goes to zero, Equation 4.42 reduces to

$$v_{AL} \int_0^{\Delta} u \mathrm{d}y = 0.5 v_{PF} \omega \left[R^2 - (H + \Delta)^2 \right] \tag{4.43}$$

In solving for the active layer depth and velocity using Equation (4.43) there are two possible constraints that may be used to terminate the iteration, that is, either by ensuring that the mass flow in the active layer is balanced at each *x*-position from the apex, using Equation (4.42), or by ensuring that global mass in the active layer is balanced at mid-chord using Equation (4.43).

4.5.6 Velocity Profile in the Active Layer

Application of integral methods for solving boundary layer flows involves fitting the velocity profile to a polynomial form

$$U = a_0 + a_1 y + a_2 y^2 \cdots + a_n y^n \tag{4.44}$$

where the degree, *n*, depends upon the number of conditions imposed on the profile by physical constraints for example stress or velocities at the boundaries. However, the experimental results indicated that a parabolic profile would be sufficient to describe the shape of the velocity profile in the active layer; hence only three conditions are imposed on the profile, (i) the free surface, (ii) the yield line which lies between the active layer and the plug flow region where deformation of material occurs, and (iii) the zero velocity line which lies between (i) and (ii) as a result of particle flow reversal.

4.5.6.1 Free Surface Boundary Condition

Following the fluid flow analogy, the most obvious choice for a free surface boundary condition is to allow the shear stresses to vanish and thereby force the shear rate to go to zero (i.e., $\mathrm{d}u/\mathrm{d}y = 0$). Although this condition has been used in chute flow calculations (Savage, 1979; Campbell and Brenen, 1985; etc.) it forces the velocity profile to a

shape that is inconsistent with the experimental results. This is consistent with instability, a condition imposed by the large particle size causing the continuum assumption to break down. Instead of null shear stress we can impose a known velocity value as this is easily measurable. The free surface velocity depends on the chord length since it is the maximum distance that a particle can travel at a certain fixed speed imposed either by the kiln rotation or by gravity (free fall). Qualitatively, the surface velocity for a bed of material with a given particle size will depend on three parameters, which are, the speed of rotation, the kiln size, and the degree of fill. A correlation equation was derived relating the surface velocity to kiln speed and fill, $u_s = C_0 \omega R$, where the constant of proportionality, C_0, was related to the degree of fill and the rotational speed of the kiln, $C_0 = f(\%\ \text{Fill};\omega)$.

4.5.6.2 Conditions at the Interface Between Plug Flow and Active Layer

At the yield line, continuity of flow in both the active layer and the plug flow region requires that $u = u_\delta$. The relationship between α and δ may be established by considering the Coulomb yield criterion, $\sigma_s = \sigma_{yy} \tan\phi$. Since $\tan\phi$ is constant, the ratio between the shear and normal stresses at the interface must also be constant. Because the normal stress is the weight of the overlying burden, the number of particles that the material can sustain between the zero line and the yield line depends on the packing and must, therefore, be related to the degree of fill. Hence, the ratio α/δ represents the yield criterion and must be a constant that is related to the percent fill. Experimental observations indicate that this is indeed true and can be used to establish the two boundary conditions. The argument is analogous to boundary layer flows where the layer depth is usually related to a certain percentage of the free stream. Gauthier (1991) gave a value of $\alpha = 0.75\delta$ for a small batch reactor using Ottawa sand as the bed material. However, it has been shown that when larger particle size ranges are involved, the ratio lies between 0.7 and 0.9 depending on the degree of fill (Boateng and Barr, 1997).

Inclusion of these constraints into the parabolic velocity profile provides an analytical expression for the profile (Appendix 4B):

$$\frac{u}{u_\delta} = \kappa + \left(\frac{\kappa\alpha^2 - \kappa\delta^2 + \alpha}{\alpha\delta^2 - \alpha^2\delta}\right) y + \left(\frac{\kappa - \kappa\alpha - \alpha}{\alpha\delta^2 - \alpha^2\delta}\right) y^2 \tag{4.45}$$

Table 4.1 Coefficients Resulting from the Velocity Profile

α/δ	a'_1	a'_2
0.75	$3.0-2.33\kappa$	$4.0-1.33\kappa$
0.80	$4.0-2.25\kappa$	$5.0-1.25\kappa$
0.85	$5.67-2.18\kappa$	$6.67-1.18\kappa$
0.90	$9.0-2.11\kappa$	$10.0-1.11\kappa$

where κ is the ratio between the velocity parallel to the bed surface, $u_s(C_0\omega R)$ and $u_\delta(\omega r_x)$, that is, $\kappa = C_0 R/r_x$. The velocity profiles for the range of values of α/δ, may be given as

$$\frac{u}{u_\delta} = \kappa + a'_1\left(\frac{y}{\delta}\right) - a'_2\left(\frac{y}{\delta}\right)^2 \tag{4.46}$$

Pertinent coefficients are presented in Table 4.1.

4.5.7 Density and Granular Temperature Profiles

The analytical model for the momentum conservation equation (Equation 4.39) applied to the active layer flow also requires density and granular temperature profiles for a solution. The density profile for the bed active layer differs from that in the plug flow region because of material dilation. In the plug flow region the solids volume concentration, ν, can be assumed to be constant and equal to the maximum shearable solids concentration, ν_*. The numerical value of ν_* depends on the material packing, which in turn depends upon the material properties and particle shape. For close packing of spherical particles, the value can be as high as 0.7. However for most practical situations it ranges between 0.59 and 0.62 (Savage, 1989). In the active layer, the solids fraction is not always constant but may vary from that of the plug flow ($\approx \nu_{PF}$) at the interface to a very small quantity, ν_0, at the free surface, as was determined for one of its components (the linear concentration profile) in the experimental results. The actual value for the solids fraction should, therefore, be determined as part of the solution of the granular flow equations because of its interdependency with the granular temperature. For the present application a linear solids concentration profile should be adequate because of the thinness of the active layer. Such an approach has been previously employed in similar calculations pertaining to sedimentation transport problems

(Hanes and Bowen, 1985). By assuming a linear solids concentration profile one can use the expression

$$\nu = \nu_* - \frac{\gamma}{\delta}(\nu_* - \nu_0) \tag{4.47}$$

Here ν_* is the "at rest" solids concentration, which should equal the packing in the plug flow region. Ideally, however, ν_0 is determined by matching the stress generated by the bed surface velocity and the stress due to the flow of freeboard gas. For sedimentation transport where vigorous saltation of particles occurs due to turbulent ocean flow, the value has been shown to range between 0.05 and 0.16 (Hanes, 1986). In the rotary kiln situation, such vigorous saltation of particles is not observed and the value of ν_0 is expected to be high for a rolling bed. Based on the experimental data, the dilation in the active layer is less than 5 percent over that in the plug flow region. Now, with respect to the granular temperature, the experimental results indicate that there is some granular conduction into the bed (Figure 4.5). Although the profile follows the same parabolic behavior as the velocity profile, it is very difficult to establish boundary conditions for the granular temperature and a reasonable isotropic value may be applied. However, with an iteration scheme, the values of granular temperature may be computed as part of the solution of the flow problem.

4.5.8 An Analytical Expression for the Thickness of the Active Layer

Substitution of the velocity profile, Equation (4.46), into the momentum conservation equation, that is, the left-hand side of Equation (4.39), and carrying out the integration yields the result

$$\frac{\mathrm{d}}{\mathrm{d}x}\rho\int_0^\delta (u^2 - u_\delta u)\mathrm{d}y = \rho\frac{\mathrm{d}}{\mathrm{d}x}\left[\left\{(\kappa^2 - \kappa) + \frac{1}{2}(2\kappa a_1' - a_1') + \frac{1}{3}(a_1'^2 - 2\kappa a_2' + a_2') - \frac{1}{4}(2a_1'a_2') + \frac{1}{5}a_2''^2\right\}\delta\right]u_\delta^2 \tag{4.48}$$

Substituting this result into Equation (4.39) yields

$$\rho\frac{\mathrm{d}}{\mathrm{d}x}\left[(b_0 + b_1\kappa + b_2\kappa^2)\delta\right]u_\delta^2 = \rho g\sin\xi + \rho_p d_p g_2(\nu)\widetilde{T}^{1/2}\frac{\mathrm{d}u}{\mathrm{d}y} \tag{4.49}$$

Table 4.2 Coefficients Resulting from the Integro-Momentum Equation

α/δ	b_0	b_1	b_2
0.75	0.170	0.422	0.033
0.80	0.177	1.875	0.0
0.85	0.093	6.768	−0.601
0.90	0.833	−0.487	−0.593

where the coefficients b_i are generated when the terms in a_i' are expanded for the various values of the ratio α/δ. Again by recognizing that $\rho = \rho_p \nu_{AL}$, Equation (4.49) becomes

$$\begin{aligned}\frac{d}{dx}\left[\left(b_0 + b_1\kappa + b_2\kappa^2\right)\delta\right]u_\delta^2 &= g\sin\xi + d_p\frac{g_2(\nu)}{\nu_{AL}}\widetilde{T}^{1/2}\frac{u_\delta}{\delta} \\ &= \frac{g\sin\xi}{u_\delta^2} + d_p\frac{g_2(\nu)\widetilde{T}^{1/2}}{\nu_{AL}u_\delta\delta}\end{aligned} \tag{4.50}$$

In Equation (4.50) (coefficients in Table 4.2), u_δ is a function of active layer depth, δ, that is, dropping the subscript, x,

$$u_\delta = \omega r\cos\theta \tag{4.51}$$

where $r = (H + \delta)/\cos\theta$ which means that the velocity at the active layer depth is given by

$$u_\delta = -\omega(H + \delta) \tag{4.52}$$

Although u_δ is a function of δ, the variables in Equation (4.50) may be separated as if the right-hand side were constant, which is consistent with the boundary layer fluid flow solution (Schlichting, 1979). In a numerical solution scheme, u_δ can be computed with a previous value of δ and then be updated. By carrying out the separation of the variables, Equation (4.50) becomes

$$\int_0^\delta \left[\left(b_0 + b_1\kappa + b_2\kappa^2\right)\delta\right]d\delta = \int_0^x \left[\frac{g\sin\xi}{u_\delta^2}\delta + d_p\frac{g_2(\nu)\widetilde{T}^{1/2}}{\nu_{AL}u_\delta}\right]dx \tag{4.53}$$

When a boundary condition, $\delta = 0|_{x=0}$ is employed at the apex (origin of flow calculation), the final form of the integral equation becomes

$$\frac{1}{2}\left(b_0 + b_1\kappa + b_2\kappa^2\right)\delta^2 - \frac{g\sin\xi}{u_\delta^2}\delta x - d_p\frac{g_2(\nu)\widetilde{T}^{1/2}}{\nu_{AL}u_\delta}x = 0 \tag{4.54}$$

This is the quadratic equation required for the prediction of the active layer depth, which in turn is substituted into the velocity profile to obtain the velocity distribution in the two-dimensional domain.

4.5.9 Numerical Solution Scheme for the Momentum Equation

The velocity determination requires the prediction of the active layer depth using Equation (4.54) at any x-position along the bed surface. It also has to be substituted into the velocity profile in order to determine the velocity parallel to the bed surface as a function of bed depth. The local velocity normal to the bed surface is then established by solving the continuity equation given in Equation (4.9). Solving for δ_x also requires the granular temperature, which is found by iteration. The value of the granular temperature obtained after convergence is an average quantity for each x-position in the active layer. The calculation scheme is given in Figure 4.12. The procedure follows the sequence whereby (i) the average granular temperature for the entire depth at any x-position is estimated; with this value $g_2(\nu)$ is computed; (ii) Equation (4.54) is solved for a first approximation of δ_x by neglecting the quadratic term; (iii) with the value of δ_x, u_δ is computed and Equation (4.54) solved for an actual value of δ_x; (iv) knowing δ_x, the velocity profile is computed, from which follows the calculation of the mass flow for the active layer at the i-position. This mass flow is compared with the value in the plug flow region at the same location using Equation (4.40) and this procedure is repeated using an improved estimate of the granular temperature if the mass flow for the active layer does not balance the mass flow in the plug flow region. Otherwise, the solution is advanced to the next i-position until mid-chord.

The stability of the solution procedure just described depends on the choice of the granular temperature needed to initiate the solution. Experiments have shown that there is an order of magnitude increase in the granular temperature for each increase in kiln speed and therefore instabilities are likely to develop when a solution for successive kiln speeds is required. Nevertheless, this problem is easily rectified by a good initial guess for the granular temperature and the choice of the mass balance convergence criterion. In order to use small convergence criteria, which are required for low granular temperatures (i.e., for low kiln speeds), small mesh sizes are required. In modeling the 1 m diameter experimental rotary apparatus, 24 nodes were used

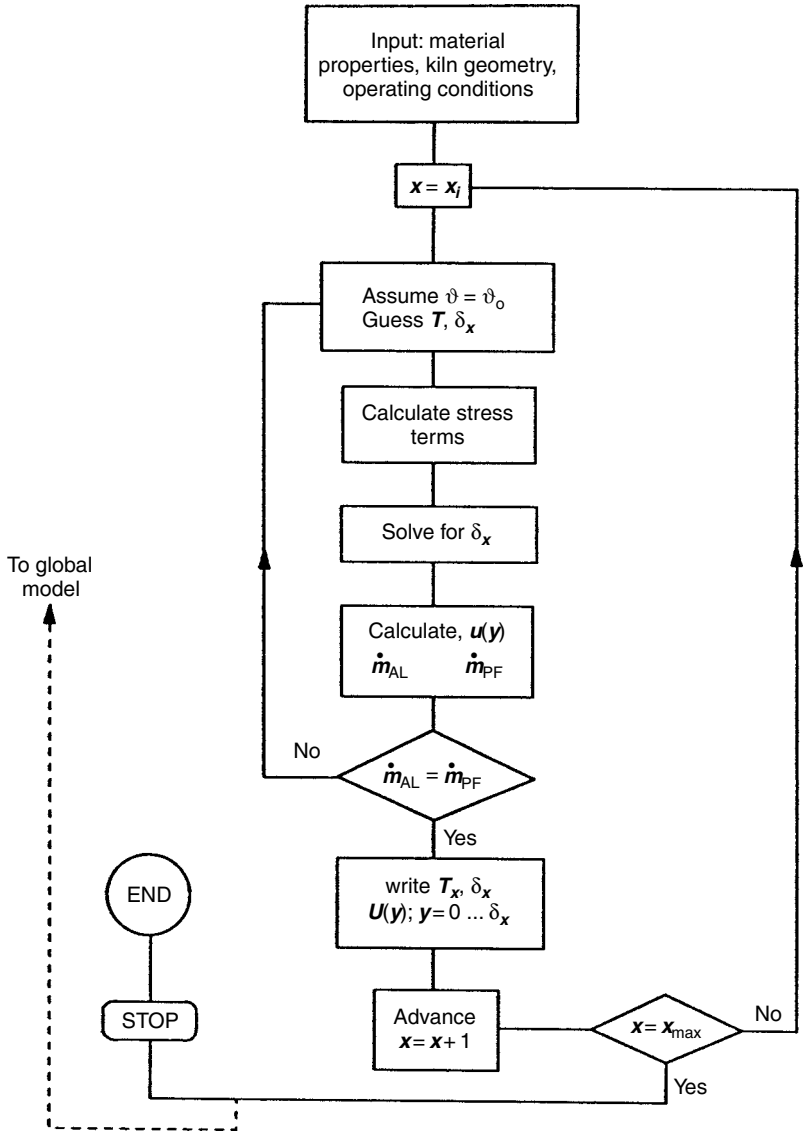

Figure 4.12 Calculation scheme for active layer depth and velocity distribution.

between the apex and the mid-chord for all the kiln speeds solved and the convergence criterion defined as the percent difference between the mass flows in the active layer and the plug flow region was set to 0.1 percent.

4.6 Model Results and Validation

The prediction of the velocity distribution for a 41 cm diameter pilot kiln is shown in Figure 4.13. Validation of the model is carried out using experimental results of the 1 m rotary drum (Figure 4.14). Here predicted and measured active layer depths are compared for the materials studied. As seen, the model underpredicts at low degree of fill

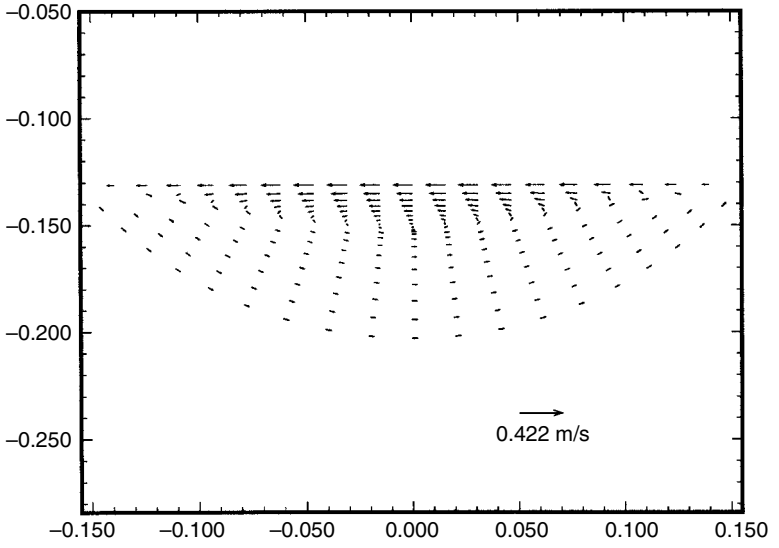

Figure 4.13 Predicted velocity distribution in the cross section of a 41 cm pilot kiln.

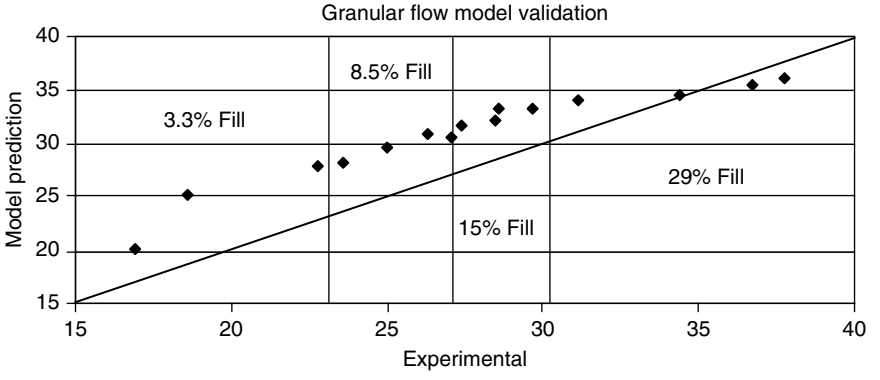

Figure 4.14 Predicted and measured active layer depth for a 1 m rotary drum.

but better agreement is achieved for deeper beds. One likely reason for the underprediction is the fact that the location of the yield line is difficult to measure in shallow beds. Aside from the bed loading, several factors affect the flow, most importantly the rheological properties of the processing materials. Some of these are presented here (Boateng, 1998). The predicted active layer velocity and depth for a 41 cm diameter pilot kiln, a 1 m diameter rotary drum, and a 2.5 m diameter industrial kiln are presented in Figures 4.15 (velocity) and 4.16 (depth).

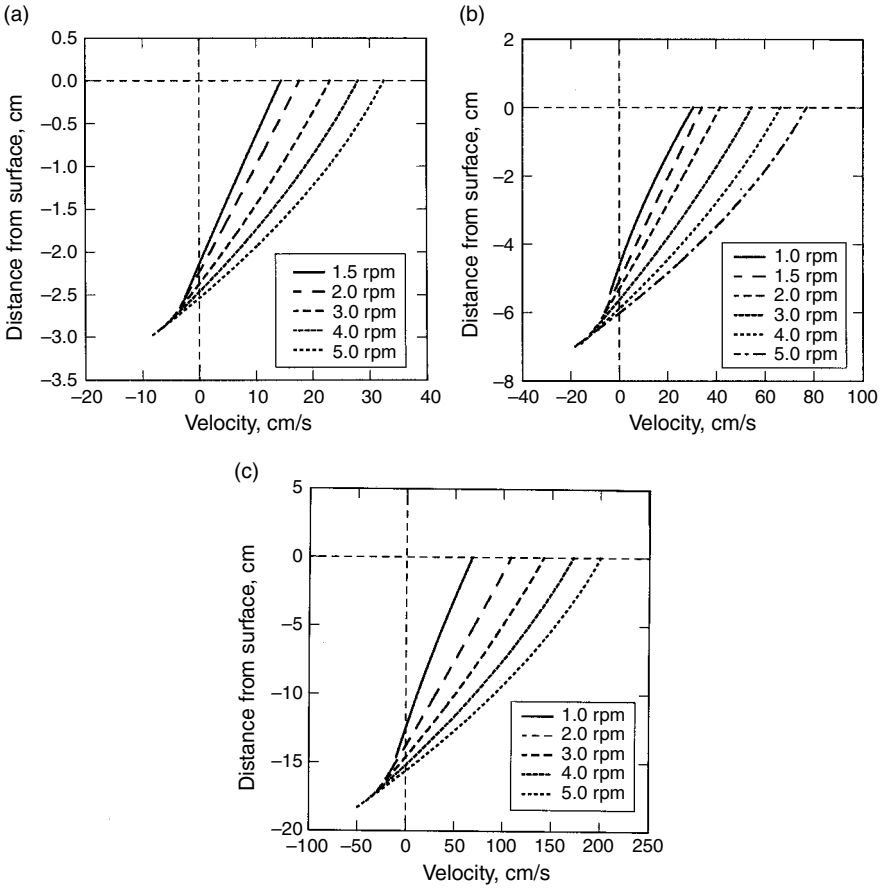

Figure 4.15 Active layer velocity as function of kiln speed. (a) 41 cm diameter pilot kiln, (b) 1 m diameter rotary drum, and (c) 2.5 m diameter industrial kiln (Boateng, 1998).

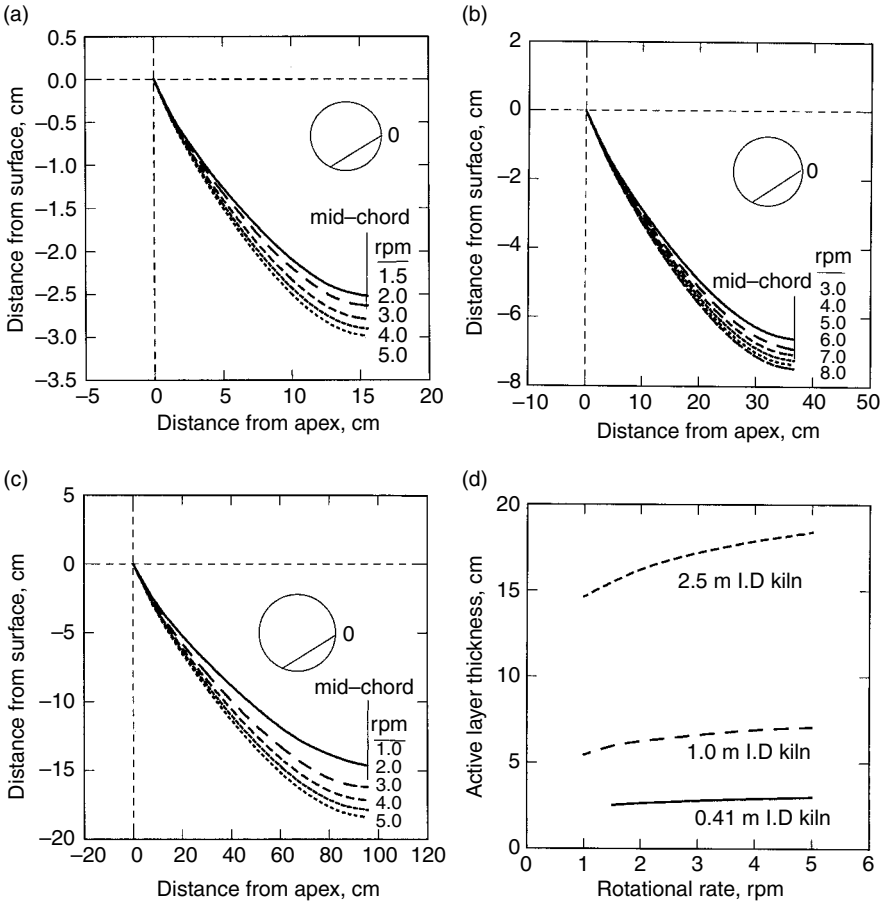

Figure 4.16 Predicted active layer depth for (a) 41 cm diameter pilot kiln, (b) 1 m diameter rotary drum, and (c) 2.5 m diameter kiln; (d) shows asymptotic nature of active layer depth with speed (Boateng, 1998).

4.7 Application of the Flow Model

The diffusion coefficient can be calculated from the predicted granular temperature as (Savage, 1983; Hsiau and Hunt, 1993)

$$\widetilde{D} = \frac{d_p \sqrt{\pi \widetilde{\widetilde{T}}}}{8\left(e_p + 1\right) \nu g_0 \left(\nu\right)} \tag{4.55}$$

The predicted results are presented in Figure 4.17. It should be noted that this provides the effect of flow or mixing on advective heat

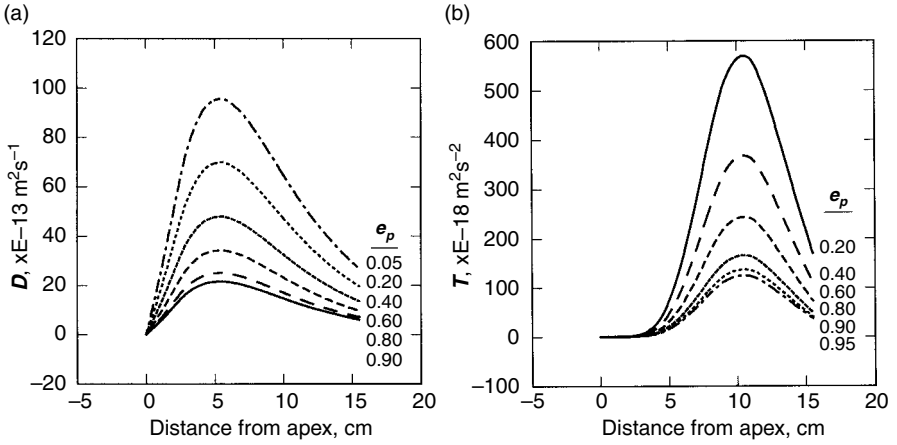

Figure 4.17 Effect of particle coefficient of restitution (e_p = 0.05–0.9) on active layer diffusion (12 percent fill, 2 rpm) (Boateng, 1998); (a) effect on granular diffusion and (b) effect on granular temperature.

transfer. The convective bed heat transfer can be calculated through knowledge of the flow field. The mass transfer enhanced thermal conductivity can be computed as $\rho c_p \widetilde{D}$ where $\widetilde{D}$, the kinetic diffusion, is computed from the granular temperature given by the flow model. Hence the enhanced bed effective thermal conductivity can be calculated (Hunt, 1997; Natarajan and Hunt, 1998) and is several orders of magnitude greater than that of a packed bed (Boateng and Barr, 1996). Previously this was not possible to estimate.

Because the active layer velocity is about three or four times greater than that in the plug flow region, mixing effects are confined to this region. However, if fine or denser particles are used as tracers, then the velocity distribution will help to determine the extent to which the tracers will travel before percolating down. These scenarios will be the subject of the next chapter.

References

H. Ahn, C. E. Brennen, and R. H. Sabersky. "Measurements of velocity, velocity fluctuation, density, and stresses in chute flows of granular materials," *J. Applied Mech.*, 58, 792–803, 1991.

R. A. Bagnold. "Experiments on a gravity-free dispersion of large solids spheres in a Newtonian fluid under shear," *Proc. R. Soc. London*, A225, 49–63, 1954.

A. A. Boateng. *Rotary Kiln Transport Phenomena: Study of the Bed Motion and Heat Transfer*. PhD Dissertation, The University of British Columbia, Vancouver, 1993.

A. A. Boateng. "Boundary layer modeling of granular flow in the transverse plane of a partially filled rotating cylinder," *Int. J. Multiphase Flow*, 24(3), 499–521, 1998.

A. A. Boateng and P. V. Barr. "A thermal model for the rotary kiln including heat transfer within the bed," *Int. J. Heat Mass Transfer*, 39(10), 2131–2147, 1996.

A. A. Boateng and P. V. Barr. "Granular flow behaviour in the transverse plane of a partially filled rotating cylinder," *J. Fluid Mech.*, 330, 233–249, 1997.

C. S. Campbell and A. Gong. "The stress tensor in a two-dimensional granular shear flow," *Fluid Mech.*, 164, 107–125, 1986.

S. C. Cowin. "A theory for the flow of granular materials," *Powder Technol.*, 9, 62–69, 1974.

T. R. H. Davies. "Large debris flow: A macro-viscous phenomenon," *Acta Mechanica*, 63, 161–178, 1986.

G. de Josselin de Jong. "Lower bound collapse theorem and lack of normality of strain rate to yield surface for soils." In *Rheology and Soil Mechanics Symposium*, Grenoble, 69–78, 1964.

J. R. Ferron and D. K. Singh. "Rotary kiln transport processes," *AIChE J.*, 37(5), 747–757, 1991.

C. Gauthier. *Etude du mouvment granulaire dans cylindre en rotation*, M.Sc. Thesis, Universite du Quebec, 1991.

D. M. Hanes. "Grain flows and bed-load sediment transport: Review and extension," *Acta Mechanica*, 63, 131–142, 1986.

D. M. Hanes and A. J. Bowen. "A granular-fluid model for steady intense bed-load transport," *J. Geophysical Research*, 90(C5), 9149–9152, 1985.

H. Henein, J. K. Brimacombe, and A. P. Watkinson. "Experimental study of transfer bed motion in rotary kilns," *Met. Trans. B*, 14B(6), 191–205, 1983a.

H. Henein, J. K. Brimacombe, and A. P. Watkinson. "The modeling of transverse solids motion in rotary kilns," *Met. Trans. B*, 14B(6), 207–220, 1983b.

S. S. Hsiau and M. L. Hunt. "Shear-induced particle diffusion and longitudinal velocity fluctuations in a granular-flow mixing layer," *J. Fluid Mech.*, 251, 299–313, 1993.

M. L. Hunt. "Discrete element simulations for granular material flows: Effective thermal conductivity and self-diffusivity," *Int. J. Heat Mass Transfer*, 40(3) 3059–3068, 1997.

P. C. Johnson and R. Jackson. "Frictional-collisional constitutive relations for granular materials, with application to plane shearing," *J. Fluid Mech.*, 176, 67–93, 1987.

K. Kanatani. "A continuum theory for the flow of granular materials," *Theoretical and Applied Mechanics*, 27, 571–578, 1979.

C. K. K. Lun, S. B. Savage, D. J. Jeffrey, and N. Chepurniy. "Kinetic theories for granular flow: Inelastic particles in couette flow and slightly inelastic particles in a general flowfield," *J. Fluid Mech.*, 140, 223–256, 1984.

G. Mandl and R. F. Luque. "Fully developed plastic shear flow of granular materials," *J. Geotechnique*, 20(3), 277–307, 1970.

M. Nakagawa, S. A. Altobelli, A. Caprihan, E. Fukushima, and E.-K. Jeong. "Non-invasive measurements of granular flows by magnetic resonance imaging," *Exp. Fluids*, 16, 54–60, 1993.

V. V. R. Natarajan and M. L. Hunt. "Kinetic theory analysis of heat transfer in granular flows," *Int. J. Heat Mass Transfer*, 41(13), 1929–1944, 1998.

D. J. Parker, A. E. Dijkstra, T. W. Martin, and J. P. K. Seville. "Positron emission particle tracking studies of spherical particle motion in rotating drums," *Chem. Eng. Sci.*, 52(13), 2011–2022, 1997.

V. F. Pershin. "Energy method for describing granular motion in a smooth rotating cylinder," *J. Teoreticheskie Osnovy Khimicheskoi Tekhnologii*, 22(2), 255–260, 1988.

K. H. Roscoe. "The influence of strains in soil mechanics," *Geotechnique*, 20, 129–170, 1970.

S. B. Savage. "Gravity flow of cohesionless granular materials in chutes and channels," *J. Fluid Mech.*, 92, 53–96, 1979.

S. B. Savage. "Granular flow down rough inclines. Review and extension." In *Mechanics of Granular Materials: New Models and Constitutive Relations* (J. T. Jenkins and M. Satake, Eds.), 261–282, Elsevier, Inc., New York, 1983.

S. B. Savage. "Granular flow materials." In *Theoretical and Applied Mechanics* (P. Germain, M. Piau, and D. Caillerie, Eds.), 241–266, Elsevier, Inc., New York, 1989.

S. B. Savage and K. Hutter. "The motion of a finite mass of granular material down a rough incline," *J. Fluid Mech.*, 199, 177–215, 1989.

H. Schlichting. *Boundary-Layer Theory*. McGraw-Hill, New York, 1979.

D. K. Singh. *A Fundamental Study of the Mixing of Solid Particles*. Ph.D. Dissertation, University of Rochester, New York, 1978.

A. J. M. Spencer. "A theory of the kinematics of ideal soils under plane strain conditions," *J. Mech. Phys. Solids*, 12, 337–351, 1964.

Y. Zhang and C. S. Campbell. "The interface between fluid-like and solid-like behaviour in two-dimensional granular flows," *J. Fluid Mech.*, 237, 541–568, 1992.

Appendix 4A

Apparent Viscosity

The term C' from the constitutive relations of Lun et al. (1984) represents the apparent viscosity if an analogy is drawn from fluid mechanics. The expression C' is derived in terms of the coefficient of restitution of the particles, the solid fraction, particle size, and the granular temperature as follows:

$$P_{xy} = \frac{\partial}{\partial y}\left(C'\frac{\partial u}{\partial y}\right) \tag{4A.1}$$

where $C' = C/2$ and,

$$C = \frac{2\mu}{\eta(2-\eta)g_0}\left(1+\frac{8}{5}\eta\nu g_0\right)\left[1+\frac{8}{5}\eta(3\eta-2)\nu g_0\right]+\frac{6}{5}\mu_b\eta \tag{4A.2}$$

and

$$\mu_b = 256\mu\nu^2 g_0/5\pi \tag{4A.3}$$

$$\mu = 5m\left(\frac{\widetilde{T}}{\pi}\right)^{1/2}\Big/16d_{\mathrm{p}}^2 \tag{4A.4}$$

$$m = \rho_{\mathrm{p}}V = \rho_{\mathrm{p}}\frac{\pi}{6}d_{\mathrm{p}}^3 \tag{4A.5}$$

Substitution of these equations into C' yields

$$C' = \frac{5\sqrt{\pi}}{96}\rho_{\mathrm{p}}d_{\mathrm{p}}\sqrt{\widetilde{T}}\left[\frac{1}{\eta(2-\eta)g_0}\left(1+\frac{8}{5}\eta\nu g_0\right)\left\{1+\frac{8}{5}\eta(3\eta-2)\nu g_0\right\}+\frac{768}{25\pi}\nu^2 g_0\right] \tag{4A.6}$$

where the term in the square bracket may be expressed as

$$C' = -g_2(\nu,\varepsilon_{\mathrm{p}})\rho_{\mathrm{p}}\sqrt{\widetilde{T}} \tag{4A.7}$$

with $g_2(\nu,\varepsilon_{\mathrm{p}})$ expressed as

$$g_2(\nu,\varepsilon_{\mathrm{p}}) = \frac{5\sqrt{\pi}}{96}\left[\frac{1}{\eta(2-\eta)g_0}+\frac{8}{5}\frac{(3\eta-1)\nu}{2-\eta}+\frac{64}{25}\left\{\frac{\eta(3\eta-2)}{2-\eta}+\frac{12}{\pi}\right\}\nu^2 g_0\right] \tag{4A.8}$$

Similarly,

$$P_{xx} = P_{xy} - \rho_p g_1(\nu, \varepsilon_p)\widetilde{T} \tag{4A.9}$$

$$q_y = -\rho_p d_p \left(g_3(\nu, \varepsilon_p)\sqrt{\widetilde{T}}\frac{d\widetilde{T}}{dy} + g_4(\nu, \varepsilon_p)\sqrt{\widetilde{T}}\frac{d\nu}{dy} \right) \tag{4A.10}$$

$$\gamma = \frac{\rho_p}{d_p} g_5(\nu, \varepsilon_p)\widetilde{T}^{3/2} \tag{4A.11}$$

where g_1 through g_5 follow (Johnson and Jackson, 1987):

$$g_0 = \left(1 - \frac{\nu}{\nu^*}\right)^{-1/3} \tag{4A.12}$$

$$g_1(\nu, \varepsilon_p) = \nu + 4\eta\nu^2 g_0 \tag{4A.13}$$

$$g_2(\nu, \varepsilon_p) = \frac{5\sqrt{\pi}}{96}\left[\frac{1}{\eta(2-\eta)g_0} + \frac{8}{5}\frac{(3\eta-1)\nu}{2-\eta} + \frac{64}{25}\left\{\frac{\eta(3\eta-2)}{2-\eta} + \frac{12}{\pi}\right\}\nu^2 g_0\right] \tag{4A.14}$$

$$g_3(\nu, \varepsilon_p) = \frac{25\pi}{16\eta(41-33\eta)}\left[\frac{1}{g_0} + \frac{12}{5\eta}\{1+\eta(4\eta-3)\}\eta + \frac{16}{25\eta^2}\left\{9\eta(4\eta-3) + \frac{4}{\pi}(41-33\eta)\right\}\nu^2 g_0\right] \tag{4A.15}$$

$$g_4(\nu, \varepsilon_p) = \frac{15\sqrt{\pi}}{4}\frac{(2\eta-1)(\eta-1)}{(41-33\eta)}\left(\frac{1}{g_0} + \frac{12\eta}{5}\right)\frac{d}{d\nu}(\nu^2 g_0) \tag{4A.16}$$

$$g_5(\nu, \varepsilon_p) = \frac{48}{\sqrt{\pi}}\eta(1-\eta)\nu^2 g_0 \tag{4A.17}$$

Appendix 4B

Velocity Profile for Flow in the Active Layer

The velocity profile with the appropriate boundary conditions is:

$$u = a_0 + a_1 y + a_2 y^2 \tag{4B.1}$$

$$\begin{aligned} &\text{at} \quad y = \alpha, \quad u = 0 \\ &\text{at} \quad y = \delta, \quad u = u_\delta \\ &\text{at} \quad y = 0, \quad u = u_s \end{aligned} \tag{4B.2}$$

Substituting these boundary conditions gives three equations, that is,

$$\begin{aligned} u_s &= a_0 \\ 0 &= a_0 + a_1\alpha + a_2\alpha^2 \\ -u_\delta &= a_0 + a_1\delta + a_2\delta^2 \end{aligned} \tag{4B.3}$$

These can be reduced to two equations

$$a_1\alpha\delta + a_2\alpha^2\delta = -u_s\delta \tag{4B.4}$$

$$a_1\alpha\delta + a_2\alpha\delta^2 = -(u_s + u_\delta)\alpha \tag{4B.5}$$

from which

$$a_1 = \frac{-u_s\delta^2 + (u_s + u_\delta)\alpha^2}{\alpha\delta^2 - \alpha^2\delta} \tag{4B.6}$$

$$a_2 = \frac{u_s\delta^2 - (u_s + u_\delta)\alpha^2}{\alpha\delta^2 - \alpha^2\delta} \tag{4B.7}$$

Substituting the coefficients gives

$$u = u_s + \frac{u_s(\alpha^2 - \delta^2) + u_\delta\alpha^2}{\alpha\delta^2 - \alpha^2\delta}y + \frac{u_s(\delta - \alpha) - u_\delta\alpha}{\alpha\delta^2 - \alpha^2\delta}y^2 \tag{4B.8}$$

Recognizing that $u_s = C_0\omega R$ and $u_\delta = \omega r_x$ yields a ratio

$$u_s = \frac{C_0R}{r_x}u_\delta = \kappa u_\delta \tag{4B.9}$$

$$\frac{u}{u_\delta} = \kappa + \frac{\kappa\alpha^2 - \kappa\delta^2 + \alpha^2}{\alpha\delta^2 - \alpha^2\delta}y + \frac{\kappa\delta - \kappa\alpha - \alpha}{\alpha\delta^2 - \alpha^2\delta}y^2 \tag{4B.10}$$

for $\alpha = 0.75\delta$

$$\frac{u}{u_\delta} = \kappa + (3 - 2.33\kappa)\left(\frac{y}{\delta}\right) - (4 - 1.33\kappa)\left(\frac{y}{\delta}\right)^2 \tag{4B.11}$$

or

$$\frac{u}{u_\delta} = \kappa + a_1'\left(\frac{y}{\delta}\right) - a_2'\left(\frac{y}{\delta}\right)^2 \tag{4B.12}$$